Friction-induced planar vibration of two rigid plates

Ningyu Liu [1,2] and Huajiang Ouyang [2] (✉)

[1] School of Traffic and Transportation Engineering, Central South University, Changsha, 410075, China

[2] School of Engineering, University of Liverpool, The Quadrangle, Liverpool L69, 3GH, U.K.

e-mail: h.ouyang@liverpool.ac.uk

Abstract

The dynamical model for friction-induced vibration of two rigid circular plates in point contact is studied in this paper. Besides the rotational motion in the circumferential direction that is normally regarded as the principal direction of relative motion, the two-dimensional translational motion is also considered for both rigid plates. The coupling of the translational motion and the rotational motion causes the direction of relative motion and friction force to shift from the circumferential direction and vary during vibration (in relation to the situation in which translational motion is absent), thereby greatly increasing the complexity of the dynamics of the friction-excited system. The system dynamics comprises two distinct states of motion, i.e., slip and stick, and the friction force during sticking is a reaction force enforcing the constraint of zero relative velocity, which cannot be explicitly expressed as a function of state variables, therefore the values of state variables and friction force in the state of stick cannot be directly obtained from the integration of equations of motion. To address this problem, two different methods are proposed and the accuracy and efficiency of the two numerical methods are subsequently examined. Both the linear stability and the nonlinear steady-state responses of the system are investigated. The numerical study demonstrates that the coupling of the translational motion and the rotational motion of the two rigid plates greatly expands the ranges of operating parameters for dynamic instability compared with those of the situation where the two rigid plates undergo only rotational motion, and results in rich bifurcation behaviours. Therefore this study underlies the necessity to take into account the oscillations of components that seem not to be in the principal direction of relative motion in the research of friction-induced vibration of mechanical systems.

Keywords: friction-induced vibration, stick-slip, coupling of translation and rotation, nonlinear contact kinematics, bifurcation.

1. Introduction

Friction-induced vibration is widely encountered in engineering and in daily life, e.g., musical sound of string instruments [1], squeaking joints of robots [2], chattering machine tools [3], stick-slip oscillations of drill strings [4] and automobile brake noise [5], etc. Among them, automobile brake noise

attracts great attention in engineering and scientific communities due to its noise impact and scientific intricacy of this problem. In essence, automobile brake noise originates from the vibration of the brake system caused by the pad-disc frictional contact in the braking process [6].

From past studies, the mechanisms for the occurrence of friction-induced vibration in mechanical systems generally fall into four categories: the negative friction slope [7], the stick-slip motion [8], the sprag-slip motion [9] and the mode-coupling instability [10]. In the mechanism of the negative friction slope, a negative damping created by the negative friction-velocity slope is thought to cause dynamic instability in the mechanical systems with friction [11]. The stick-slip motion is characterized by alternating stick and slip regimes brought about by the non-smooth nature of dry friction. Popp et al. [12,13] studied discrete and continuous models exhibiting friction-induced stick-slip vibration. Ouyang et al. [14,15] investigated the stick-slip-separation vibration of mass-slider-on-rotating-disc models under the constant and time-varying disc speed. Lin [16] presented a numerical study of stick-slip mitigation for a lumped-parameter drill-string system. The sprag-slip is not a tribological but a geometrical instability. Hoffmann et al. [17,18] found that the frictional system having no static solution for certain parameter values could be a sufficient condition for the occurrence of sprag-slip instability by examining the dynamics of a tilted-beam-moving-belt model. In the mechanism of mode-coupling instability, the complex eigenvalue analysis shows that some modes become unstable when coupling with other modes of the friction system. Hoffmann et al. [19,20] clarified the physical mechanism underlying the mode-coupling instability and the effect of viscous damping on the mode-coupling instability, respectively. Hervé et al. [21] analysed the effects of the gyroscopic actions on the mode-coupling instability. A combination of different mechanisms for friction-induced vibration may be seen in a mechanical system with friction. Elmaian et al. [22] investigated the friction-induced vibration of a 3-DoF (degree-of-freedom) model that displayed the stick-slip, the sprag-slip and mode-coupling instabilities and the links of different instability mechanisms with different categories of noises. Liu and Ouyang [23] analysed the suppression of friction-induced vibration caused by three factors, i.e. the negative friction slope, the mode coupling instability and the effect of moving load.

Friction-induced vibration in mechanical systems can exhibit rich dynamic behaviours, e.g., bifurcations, chaos, non-stationary effect, etc. Popp and Stelter [24] analysed the bifurcation behaviours of the stick-slip oscillations of a 1-DoF slider-on-belt system under external harmonic excitation and a 2-DoF slider-on-belt system. Li and Feng [25] found that chaotic motions could appear in even a 1-DoF system with the LuGre friction model containing one internal variable. Weiss et al. [26] studied the stability behaviour and the post bifurcation behaviour of the resulting limit cycle of a ball joint subject to friction-induced oscillations. Kruse et al. [27] explored the effect of joints on the stability and bifurcation behaviour of friction-induced flutter. It was shown that subcritical bifurcations, bifurcations from infinity and detached limit cycles could arise when the joint with nonlinear dynamic behaviour is integrated in the system. Wei et al. [28] established a 3-DoF dynamic model of a brake system consisting

of two-layer pads and a rigid disc and bifurcation and chaotic behaviours of system responses dependent on the variations of brake pressure and the parameters of pads were observed. Liu et al. [29] investigated the multi-stable characteristics of the torsional stick-slip vibrations in a lumped-parameter model of the drill-string system. Pilipchuck et al. [30] examined the non-stationary effects in friction-induced vibration of a 2-DoF slider-on-belt model with linearly decreasing belt speed. Liu and Ouyang [31] analysed the bifurcation behaviours in the friction-induced vibration of a 5-DoF dynamic model with multiple types of nonlinearities. Papangelo et al. [32] explored multiple spatially localized dynamical states occurring in a 'snake-like' bifurcation pattern in a chain of friction-excited oscillators.

In the existing studies on friction-induced vibration, the directions of friction force are usually known a priori, e.g., the horizontal direction in the friction model with a moving belt, or the circumferential direction in the friction model with a rotating disc, in the assumption that the oscillations in other directions are negligible. However, due to the factors such as external disturbance, manufacturing errors, non-rigid connections, etc, in engineering practices, oscillations of a frictional system may happen in any direction and therefore cause the direction of friction force to vary with time, which then further increases the complexity of the dynamics of the friction-excited system. In view of the above, it is essential to consider the direction of vibration to be unknown a priori and to be determined when studying the friction-induced dynamics of some mechanical systems. Kinkaid et al. [33] studied the dynamics of a 4-DoF system with a two-dimensional friction force and found the change of direction of the friction force could excite unstable vibration. Antali and Stepan [34] examined the dynamics of a rigid body in three-dimensional sliding or rolling contact with a rigid plane in the presence of dry friction. Ma and Wang [35] dealt with planar multiple-contact problems subject to unilateral and bilateral kinetic constraints with static Coulomb friction. Charroyer et al. [36,37] studied the self-excited vibration of a non-smooth contact dynamical system with planar friction. Lisowski et al. [38] identified the nonlinear dynamics of the double torsion pendulum with planar friction and elastic barriers.

Xia [39] investigated the dynamics of a model of wedge dampers of trucks in the presence of two-dimensional dry friction. Sanliturk and Ewins [40] presented an approach to the modelling of two-dimensional behaviour of a point friction contact which facilitated the computation of the nonlinear dynamic response of a structure with joints constrained by friction. Menq et al. [41] put forward an approximate method for analysing the dynamic responses of structures having a two-dimensional frictional constraint. As an extension to the above studies, this paper proposes a novel dynamical model composed of two rigid circular plates in point frictional contact and investigates its dynamics. In this new dynamic model, the translational motion couples with the rotational motion for both rigid plates through friction so that nonlinear kinematics of the frictional contact is resulted. The responses of the present model are compared with the results of the reduced model of only rotation for studying friction-

induced vibration, i.e., in the reduced model the centres of the two rigid plates are rigidly constrained and therefore there is only rotational motion of plates around their respective centres.

The rest of the paper is arranged as follows. In Section 2 the mechanical model is introduced and the equations of motion for the system in two distinct states, i.e., slip and stick, are derived. The conditions for the transitions between the two states are determined. In Section 3 the numerical algorithms to calculate the transient dynamic responses of the system are established. In Section 4 the numerical study of the linear stability and nonlinear steady-state responses of the system is conducted. Finally in Section 5 the important conclusions are drawn.

2. Mechanical model and dynamic equations

The model of the proposed frictional system is shown in Fig. 1, which consists of two rigid circular plates in point frictional contact. The upper rigid plate, which is stationary initially, is elastically constrained at its centre O_1 by two translational springs k_{px} and k_{py} in the directions of x_1 and y_1, and to its centre by torsional spring $k_{\mathrm{p}\phi}$ in the circumferential direction, respectively. The lower rigid plate, which rotates at the angular velocity Ω, is elastically constrained at its centre O_2 by two translational springs k_{dx} and k_{dy} in the directions of x_2 and y_2, and to its centre by torsional spring $k_{\mathrm{d}\psi}$ in the circumferential direction. The two plates are preloaded by a normal compressive force N to be in point contact at the distance r to the centre O_1. The friction force generated at the point contact P will cause planar vibrations of both rigid plates and will itself fluctuate in a complicated manner too. Points O_1 and O_2 have identical planar coordinates initially.

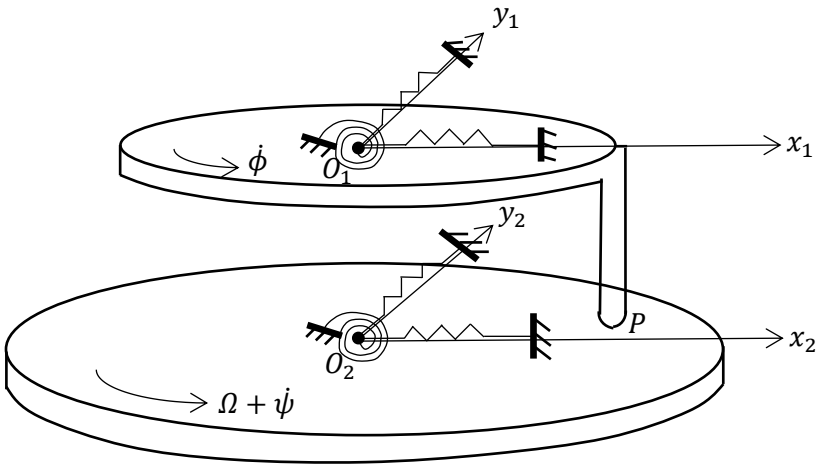

Fig. 1 The model of the frictional system.

In Fig. 2, the nonlinear kinematics of the frictional contact of the two plates during vibration is illustrated, where the axes $\mathbf{e}_x$ and $\mathbf{e}_y$ are fixed in space, $\mathbf{e}_{\mathrm{n}_1}$ and $\mathbf{e}_{\mathrm{n}_2}$ represent the unit vectors of the velocities of the upper and lower plate at the contact point, respectively. And the equations of motion of the system can be written as,

$$\begin{cases} m_{\mathrm{p}}\ddot{x}_1 + c_{\mathrm{px}}\dot{x}_1 + k_{\mathrm{px}}x_1 = \mathbf{F}_{\mathrm{f}} \cdot \mathbf{e}_x \\ m_{\mathrm{p}}\ddot{y}_1 + c_{\mathrm{py}}\dot{y}_1 + k_{\mathrm{py}}y_1 = \mathbf{F}_{\mathrm{f}} \cdot \mathbf{e}_y \\ m_{\mathrm{d}}\ddot{x}_2 + c_{\mathrm{dx}}\dot{x}_2 + k_{\mathrm{dx}}x_2 = -\mathbf{F}_{\mathrm{f}} \cdot \mathbf{e}_x \\ m_{\mathrm{d}}\ddot{y}_2 + c_{\mathrm{dy}}\dot{y}_2 + k_{\mathrm{dy}}y_2 = -\mathbf{F}_{\mathrm{f}} \cdot \mathbf{e}_y \\ J_{\mathrm{p}}\ddot{\phi} + c_{\mathrm{p}\phi}\dot{\phi} + k_{\mathrm{p}\phi}\phi = r\mathbf{F}_{\mathrm{f}} \cdot \mathbf{e}_{\mathrm{n}_1} \\ J_{\mathrm{d}}\ddot{\psi} + c_{\mathrm{d}\psi}\dot{\psi} + k_{\mathrm{d}\psi}\psi = -R\mathbf{F}_{\mathrm{f}} \cdot \mathbf{e}_{\mathrm{n}_2} \end{cases} \tag{1}$$

where m_{p}, J_{p} and m_{d}, J_{d} are the mass and rotational inertia of the upper and lower rigid plates, respectively, c_{px}, c_{py}, c_{dx}, c_{dy}, $c_{\mathrm{p}\phi}$, $c_{\mathrm{d}\psi}$ represent the viscous damping in parallel with the corresponding translational and torsional springs. R is the distance between the contact point and the centre of the lower rigid plate, which is,

$$R = \sqrt{(x_1 - x_2 + r\cos\phi)^2 + (y_1 - y_2 + r\sin\phi)^2} \tag{2}$$

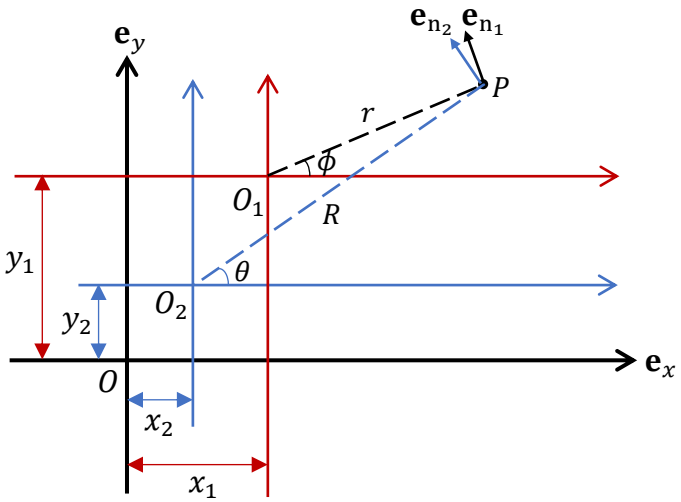

Fig. 2 The schematic plot of the position of contact point during vibration.

$\mathbf{F}_{\mathrm{f}} = F_{\mathrm{fx}}\mathbf{e}_x + F_{\mathrm{fy}}\mathbf{e}_y$ is the friction force between the two plates, which, in the state of slip ($\mathbf{v}_{\mathrm{r}} \neq \mathbf{0}$), can be formulated as,

$$\mathbf{F}_{\mathrm{f}} = -\mu(\|\mathbf{v}_{\mathrm{r}}\|)N\frac{\mathbf{v}_{\mathrm{r}}}{\|\mathbf{v}_{\mathrm{r}}\|} \tag{3}$$

where $\mu(\|\mathbf{v}_{\mathrm{r}}\|)$ represents the coefficient of kinetic friction that is a function of relative velocity, and a popular expression of $\mu(\|\mathbf{v}_{\mathrm{r}}\|)$ formulated as an exponential decay function is employed here [42], i.e.,

$$\mu(\|\mathbf{v}_{\mathrm{r}}\|) = \mu_{\mathrm{k}} + \Delta\mu \mathrm{e}^{-\alpha\|\mathbf{v}_{\mathrm{r}}\|} \tag{4}$$

where $\Delta\mu = \mu_{\mathrm{s}} - \mu_{\mathrm{k}}$, μ_{k} and μ_{s} are the asymptotic value and maximum value of the friction coefficient, α is the exponential decay factor, $\mathbf{v}_{\mathrm{r}}$ is the relative velocity between the two plates at the contact point, namely, $\mathbf{v}_{\mathrm{r}} = \mathbf{v}_{\mathrm{c}}^{\mathrm{p}} - \mathbf{v}_{\mathrm{c}}^{\mathrm{d}}$, and,

$$\mathbf{v}_{\mathrm{c}}^{\mathrm{p}} = \dot{x}_1\mathbf{e}_x + \dot{y}_1\mathbf{e}_y + \dot{\phi}r\mathbf{e}_{\mathrm{n}_1} \tag{5}$$

$$\mathbf{v}_{\mathrm{c}}^{\mathrm{d}} = \dot{x}_2\mathbf{e}_x + \dot{y}_2\mathbf{e}_y + \left(\Omega + \dot{\psi}\right)R\mathbf{e}_{\mathrm{n}_2} \tag{6}$$

The unit vectors $\mathbf{e}_{\mathrm{n}_1}$ and $\mathbf{e}_{\mathrm{n}_2}$ can be expressed as,

$$\mathbf{e}_{\mathrm{n}_1} = -\sin\phi\mathbf{e}_x + \cos\phi\mathbf{e}_y \tag{7}$$

$$\mathbf{e}_{\mathrm{n}_2} = -\sin\theta\mathbf{e}_x + \cos\theta\mathbf{e}_y = -\frac{y_1 - y_2 + r\sin\phi}{R}\mathbf{e}_x + \frac{x_1 - x_2 + r\cos\phi}{R}\mathbf{e}_y \tag{8}$$

By substituting Eqs. (5)-(8) into the expression of $\mathbf{v}_{\mathrm{r}}$, it is obtained that,

$$\mathbf{v}_{\mathrm{r}} = \left[\dot{x}_1 - \dot{x}_2 - r\dot{\phi}\sin\phi + \left(\Omega + \dot{\psi}\right)(y_1 - y_2 + r\sin\phi)\right]\mathbf{e}_x + \left[\dot{y}_1 - \dot{y}_2 + r\dot{\phi}\cos\phi - \left(\Omega + \dot{\psi}\right)(x_1 - x_2 + r\cos\phi)\right]\mathbf{e}_y \tag{9}$$

In the state of stick, the friction force serves to sustain the relative static state, i.e., $\mathbf{v}_{\mathrm{r}} = \mathbf{0}$, and thus can be obtained from the dynamic equations of the system, Eq. (1). As both $\mathbf{v}_{\mathrm{c}}^{\mathrm{p}}$ and $\mathbf{v}_{\mathrm{c}}^{\mathrm{d}}$ during sticking are unknown a priori, a new method to derive the values of the state variables and the friction force in the state of stick must be proposed. The condition for the system to stay in the state of stick is,

$$\|\mathbf{F}_{\mathrm{f}}\| \leq \mu_{\mathrm{s}}N \tag{10}$$

Therefore, at the time instant when the condition Eq. (10) is violated, the transition from stick to slip happens and the friction force will be governed by Eq. (3); at the time instant when $\mathbf{v}_{\mathrm{r}} = \mathbf{0}$ and the condition Eq. (10) is satisfied, the transition from slip to stick occurs and the value of friction force will be obtained from the dynamic equations of the system, and the method proposed in Section 3.

3. Mathematical Treatment

The friction force in the state of slip is an explicit function of the state variables, therefore the equations of motion of the system during slipping are standard ordinary differential equations (ODEs) which can be integrated by the fourth-order Runge-Kutta algorithm [43] with good accuracy. However, the friction force during sticking is a reaction force enforcing $\mathbf{v}_{\mathrm{r}} = \mathbf{0}$, which is not explicitly expressed as the function of state variables, therefore the equations of motion of the system during sticking cannot be directly integrated. Here, two methods to determine the values of the state variables and the friction force in the state of stick are presented.

In the first method, $\mathbf{v}_{\mathrm{r}} = \mathbf{0}$ results in the following relations of the state variables during sticking as,

$$\begin{cases} \dot{x}_2 = \dot{x}_1 - r\dot{\phi}\sin\phi + \left(\Omega + \dot{\psi}\right)(y_1 - y_2 + r\sin\phi) \\ \dot{y}_2 = \dot{y}_1 + r\dot{\phi}\cos\phi - \left(\Omega + \dot{\psi}\right)(x_1 - x_2 + r\cos\phi) \\ \ddot{x}_2 = \ddot{x}_1 - r\left(\ddot{\phi}\sin\phi + \dot{\phi}^2\cos\phi\right) + \left(\dot{\Omega} + \ddot{\psi}\right)(y_1 - y_2 + r\sin\phi) + \left(\Omega + \dot{\psi}\right)\left(\dot{y}_1 - \dot{y}_2 + r\dot{\phi}\cos\phi\right) \\ \ddot{y}_2 = \ddot{y}_1 + r\left(\ddot{\phi}\cos\phi - \dot{\phi}^2\sin\phi\right) - \left(\dot{\Omega} + \ddot{\psi}\right)(x_1 - x_2 + r\cos\phi) - \left(\Omega + \dot{\psi}\right)\left(\dot{x}_1 - \dot{x}_2 - r\dot{\phi}\sin\phi\right) \\ x_2(t) = x_1(t) + \int_{t_{\mathrm{s}}}^{t}\left[-r\dot{\phi}\sin\phi + \left(\Omega + \dot{\psi}\right)(y_1 - y_2 + r\sin\phi)\right]\mathrm{d}t + x_2(t_{\mathrm{s}}) - x_1(t_{\mathrm{s}}) \\ y_2(t) = y_1(t) + \int_{t_{\mathrm{s}}}^{t}\left[r\dot{\phi}\cos\phi - \left(\Omega + \dot{\psi}\right)(x_1 - x_2 + r\cos\phi)\right]\mathrm{d}t + y_2(t_{\mathrm{s}}) - y_1(t_{\mathrm{s}}) \end{cases} \tag{11}$$

where t_s is the time at the onset of stick. Given that very small time steps are used in the simulation of dynamic responses during sticking, the trapezoidal integration rule [44] is applied to calculate the values of the state variables x_2 and y_2 in Eq. (11).

The trapezoidal integration rule is a basic and popular method of numerical integration and has been widely used in numerical analysis, when it is necessary to adopt appropriate step lengths to guarantee the accuracy. There are also strategies proposed for the trapezoidal integration method to achieve good accuracy with low computation cost [45-49]. By means of the trapezoidal integration rule, the following equations are resulted,

$$(x_2 - x_1)_{t_n} = \frac{\Lambda - \frac{\Delta t}{2}(\Omega+\dot{\psi})_{t_n}\Pi}{1+\frac{\Delta t^2}{4}(\Omega+\dot{\psi})_{t_n}^2},\ (y_2 - y_1)_{t_n} = \frac{\frac{\Delta t}{2}(\Omega+\dot{\psi})_{t_n}\Lambda + \Pi}{1+\frac{\Delta t^2}{4}(\Omega+\dot{\psi})_{t_n}^2} \tag{12}$$

where

$$\Lambda = (x_2 - x_1)_{t_{n-1}} + \frac{\Delta t}{2}\left[\left(-r\dot{\phi}\sin\phi + (\Omega+\dot{\psi})(y_1 - y_2 + r\sin\phi)\right)_{t_{n-1}} + \left(-r\dot{\phi}\sin\phi + r(\Omega+\dot{\psi})\sin\phi\right)_{t_n}\right]$$

$$\Pi = (y_2 - y_1)_{t_{n-1}} + \frac{\Delta t}{2}\left[\left(r\dot{\phi}\cos\phi - (\Omega+\dot{\psi})(x_1 - x_2 + r\cos\phi)\right)_{t_{n-1}} + \left(r\dot{\phi}\cos\phi - r(\Omega+\dot{\psi})\cos\phi\right)_{t_n}\right]$$

and $(\cdot)_{t_{n-1}}$, $(\cdot)_{t_n}$ are the values of the quantities in the parentheses at time instants t_{n-1} and t_n during sticking, respectively; $\Delta t = t_n - t_{n-1}$. From Eqs. (11) and (12), the values of x_2, y_2 and their derivatives at the current time instant can be obtained from the values of other state variables at the current time instant and the values of state variables at the previous time instant, in the state of stick. Besides, the equations of motion of the system, i.e., Eq. (1), can be rewritten as,

$$\begin{cases} m_p\ddot{x}_1 + m_d\ddot{x}_2 + c_{px}\dot{x}_1 + c_{dx}\dot{x}_2 + k_{px}x_1 + k_{dx}x_2 = 0 \\ m_p\ddot{y}_1 + m_d\ddot{y}_2 + c_{py}\dot{y}_1 + c_{dy}\dot{y}_2 + k_{py}y_1 + k_{dy}y_2 = 0 \\ J_p\ddot{\phi} + c_{p\phi}\dot{\phi} + k_{p\phi}\phi - r\left[(m_p\ddot{y}_1 + c_{py}\dot{y}_1 + k_{py}y_1)\cos\phi - (m_p\ddot{x}_1 + c_{px}\dot{x}_1 + k_{px}x_1)\sin\phi\right] = 0 \\ J_d\ddot{\psi} + c_{d\psi}\dot{\psi} + k_{d\psi}\psi + R\left[(m_p\ddot{y}_1 + c_{py}\dot{y}_1 + k_{py}y_1)\frac{x_1 - x_2 + r\cos\phi}{R} - (m_p\ddot{x}_1 + c_{px}\dot{x}_1 + k_{px}x_1)\frac{y_1 - y_2 + r\sin\phi}{R}\right] = 0 \end{cases} \tag{13}$$

Then, by substituting Eqs. (11) and (12) into Eq. (13), the original 6-DoF equations of motion involving x_1, y_1, x_2, y_2, ϕ, ψ and their derivatives are converted into a 4-DoF equations of motion involving x_1, y_1, ϕ, ψ and their derivatives in the state of stick. By integrating the 4-DoF equations of motion, the values of x_1, y_1, ϕ, ψ (also including their derivatives) during sticking are determined, and the values of x_2, y_2 (also including their derivatives) during sticking can also be acquired from Eqs. (11) and (12). Besides, the components F_{fx} and F_{fy} of the friction force during sticking can be obtained from the first and second equation (or the third and fourth equation) in Eq. (1).

In the second method, as the friction force during sticking can be regarded as a Lagrange multiplier enforcing the constraint $\mathbf{v}_r = \mathbf{0}$, various values of F_{fx} and F_{fy} can be tried when integrating the equations of motion (i.e., Eq. (1)) until F_{fx} and F_{fy} that enable $\mathbf{v}_r = \mathbf{0}$ are found, which are exactly the

values of F_{fx} and F_{fy} during sticking. And the values of the state variables during sticking can be obtained simultaneously by integration. Unlike those in the first method, the equations of motion do not have to be alternated between the states of slip and stick, but multiple times of integrations need to be done at each time step in the state of stick in order to find the accurate value of friction force.

The conditions for the transition of states are monitored at each time step of the numerical algorithms. Within the time step in which the transition of states occurs, the bisection method is employed to capture the precise time instant of transition. After the transition point, the state changes and in the first method, the equations of motion switch, while in the second method, only the friction force is obtained differently. For the sake of differentiation, the first and the second numerical method can also be named 'method of alternated equations of motion (AEOM method)' and 'method of no alternated equations of motion (NAEOM method)', respectively.

4. Numerical study

4.1 Stability analysis

The stability of the equilibrium point of the system, i.e., the steady sliding state, is analysed, which can be used for the initial estimation of unstable modes that possibly lead to self-excited vibration. The procedure to carry out the stability analysis is as follows.

Firstly, the nonlinear algebraic equations whose solution is the equilibrium point are obtained,

$$\mathbf{K}\mathbf{x} = \mathbf{b} \tag{14}$$

where $\mathbf{x} = [x_1, y_1, x_2, y_2, \phi, \psi]^{\mathrm{T}}$, $\mathbf{K} = \mathrm{diag}\left(k_{\mathrm{px}}, k_{\mathrm{py}}, k_{\mathrm{dx}}, k_{\mathrm{dy}}, k_{\mathrm{p}\phi}, k_{\mathrm{d}\psi}\right)$, $\mathbf{b} = [b_1, b_2, b_3, b_4, b_5, b_6]^{\mathrm{T}}$, and the expressions of components b_i $(i = 1,2,3,4,5,6)$ are given in the Appendix. By solving Eq. (14), the equilibrium point of the system can be found.

Then, a linearized system is derived by linearizing the equations of motion of the system, i.e., Eq. (1), around the equilibrium point, namely,

$$\mathbf{M}_{\mathrm{L}}\ddot{\bar{\mathbf{x}}} + \mathbf{C}_{\mathrm{L}}\dot{\bar{\mathbf{x}}} + \mathbf{K}_{\mathrm{L}}\bar{\mathbf{x}} = \mathbf{0} \tag{15}$$

where $\bar{\mathbf{x}} = \mathbf{x} - \mathbf{x}_{\mathrm{e}}$, $\mathbf{x}_{\mathrm{e}} = [x_{1\mathrm{e}}, y_{1\mathrm{e}}, x_{2\mathrm{e}}, y_{2\mathrm{e}}, \phi_{\mathrm{e}}, \psi_{\mathrm{e}}]^{\mathrm{T}}$ represents the equilibrium point. The entries in the matrices $\mathbf{M}_{\mathrm{L}}$, $\mathbf{C}_{\mathrm{L}}$ and $\mathbf{K}_{\mathrm{L}}$ are also provided in the Appendix. The eigenvalues of the linearized system are subsequently obtained. Negative real parts of all the eigenvalues indicate a stable equilibrium point, while positive real parts of at least one of the eigenvalues indicate unstable equilibrium point and occurrence of friction-induced self-excited vibration in the system.

In the numerical analysis, the structural parameters are assigned with values in Table 1 if not specified otherwise. Fig. 3 shows the ranges of operating parameters N and Ω leading to a stable and unstable equilibrium point of the system. It is observed that the equilibrium point of the system is unstable at sufficiently low Ω and large N. Besides, $\Delta\mu$ and α also have significant effects on the

stability of the equilibrium point of the system, specifically, the increase of $\Delta\mu$ and α expands and narrows the range of operating parameters (N, Ω) for instability, respectively. In Fig. 4, the results of linear stability analysis of the present model are compared with those of the reduced model in which the two rigid plates have no translational motion but only rotational motion, which show that the unstable ranges of (N, Ω) (i.e., the values of parameters leading to an unstable equilibrium point) of the present model are significantly larger than those of the reduced model. That is to say, the nonlinear kinematics of contact brought about by the coupling of translational motion and rotational motion of the two rigid plates promotes the occurrence of dynamic instability.

Table 1 The values of structural parameters in the numerical analysis

m_{p}	m_{d}	J_{p}	J_{d}	c_{px}	k_{px}	c_{py}	k_{py}	c_{dx}
1kg	10kg	0.5kg·m^2	5kg·m^2	0.1N·s/m	300N/m	0.1N·s/m	300N/m	0.1N·s/m
k_{dx}	c_{dy}	k_{dy}	$c_{\mathrm{p}\phi}$	$k_{\mathrm{p}\phi}$	$c_{\mathrm{d}\psi}$	$k_{\mathrm{d}\psi}$	r	
3000N/m	0.1N·s/m	3000N/m	0.1N·m·s	100N·m	0.1N·m·s	1000N·m	0.2m	

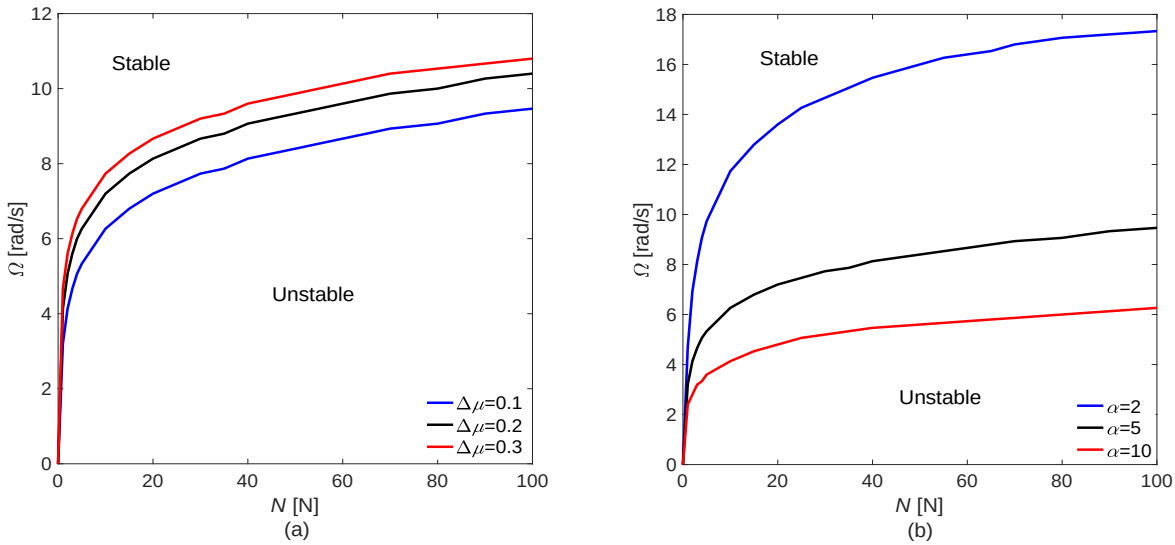

Fig. 3 The ranges of operating parameters (N, Ω) leading to stable and unstable equilibrium point of the system with : (a) $\Delta\mu = 0.1, 0.2, 0.3$, $\alpha = 5$ and (b) $\alpha = 2, 5, 10$, $\Delta\mu = 0.1$. ($\mu_{\mathrm{k}} = 0.2$).

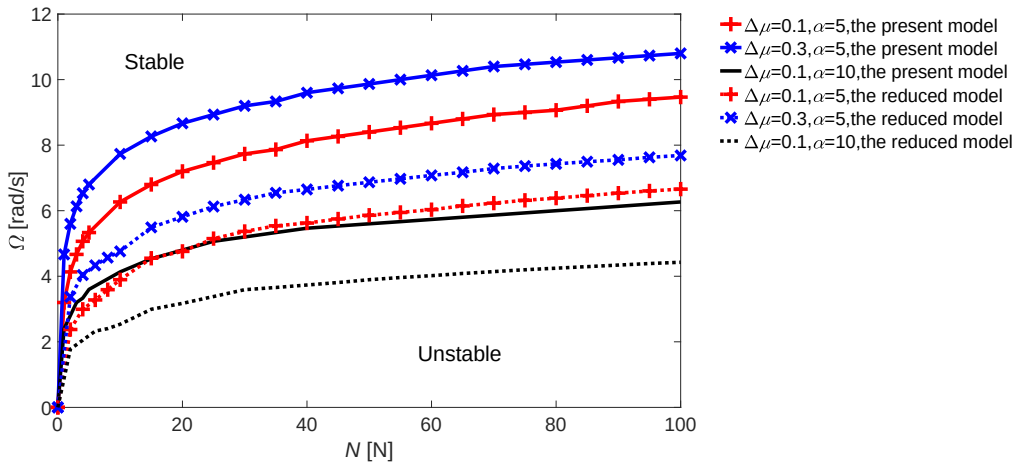

Fig. 4 The ranges of operating parameters (N, Ω) leading to stable and unstable equilibrium point of the system of the present model and the reduced model. ($\mu_{\mathrm{k}} = 0.2$).

4.2 Transient dynamic analysis

In this section, the steady-state responses of this nonlinear friction-excited system are investigated by means of the transient dynamic analysis with the two numerical methods in Section 3. The values of the structural parameters are the same as those in Table 1.

4.2.1 The accuracy and efficiency of numerical methods

The accuracy and efficiency of the two numerical methods for the calculation of the transient dynamics of the system are firstly examined. For both numerical methods, there exist numerical errors accumulated by using Runge-Kutta algorithm to integrate the differential equations. In the AEOM method, there are extra numerical errors produced when applying the trapezoidal integral rule for the integration of Eq. (11) in order to obtain the values of the state variables and the friction force in the state of stick. In the NAEOM method, however, the unknown friction force during sticking can be precisely obtained, though multiple trials of integrations have to be done to find the values of the friction force enabling the constraint of stick at every time step, which is time-consuming. Therefore, the NAEOM method has an advantage in accuracy but a disadvantage in efficiency over the AEOM method. In the following, the accuracy and efficiency of the two numerical methods are examined in a numerical example In Figs. 5 and 6, the steady-state responses of ϕ and $\|\mathbf{F}_{\mathrm{f}}\|$ for $\Omega = 5\mathrm{rad/s}$, $N = 50\mathrm{N}$, $\mu_{\mathrm{k}} = 0.2$, $\Delta\mu = 0.1$, $\alpha = 5$ calculated by the two numerical methods with various time steps are shown. In both figures, it is found that the steady-state responses with $\Delta t = 0.0001\mathrm{s}$ and $\Delta t = 0.00001\mathrm{s}$ are nearly the same, which, however, are quite different from the results with $\Delta t = 0.001\mathrm{s}, 0.01\mathrm{s}, 0.1\mathrm{s}$. Therefore, the accuracy of results obtained by the two numerical methods can only be guaranteed when sufficiently small time steps are used. Besides, it is observed from Figs. 5 and 6 that the results calculated by the AEOM method are almost identical to the results obtained from the NAEOM method , which thus demonstrates the credibility of the results from the AEOM method.

The time costs of the computation of transient dynamic responses (0~100s) by the two numerical methods with various time steps are given in Table 2. When $\Delta t = 0.1\text{s}$ or 0.01s, there are no sticking phases in the results from either numerical method, hence the same computation time is taken by the two numerical methods. When $\Delta t = 0.001\text{s}$, 0.0001s or 0.00001s, the sticking phases are found, and described in Table 2. The computation time taken by the NAEOM method is much longer than that by the AEOM method, which indicates that the AEOM method is much more efficient than the NAEOM method.

In addition, the computations of dynamic responses of the system by the two numerical methods with various time steps are also done for many other sets of parameter values, from which similar observations to those in the above example are made, i.e., (1) for both numerical methods, sufficiently small time steps need to be employed to obtain accurate results; (2) the results calculated by the AEOM method are nearly equal to the results obtained by the NAEOM method when the time step is small; (3) the AEOM method has much higher efficiency than the NAEOM method. For these reasons, it is preferable to conduct the transient dynamic analysis by the AEOM method.

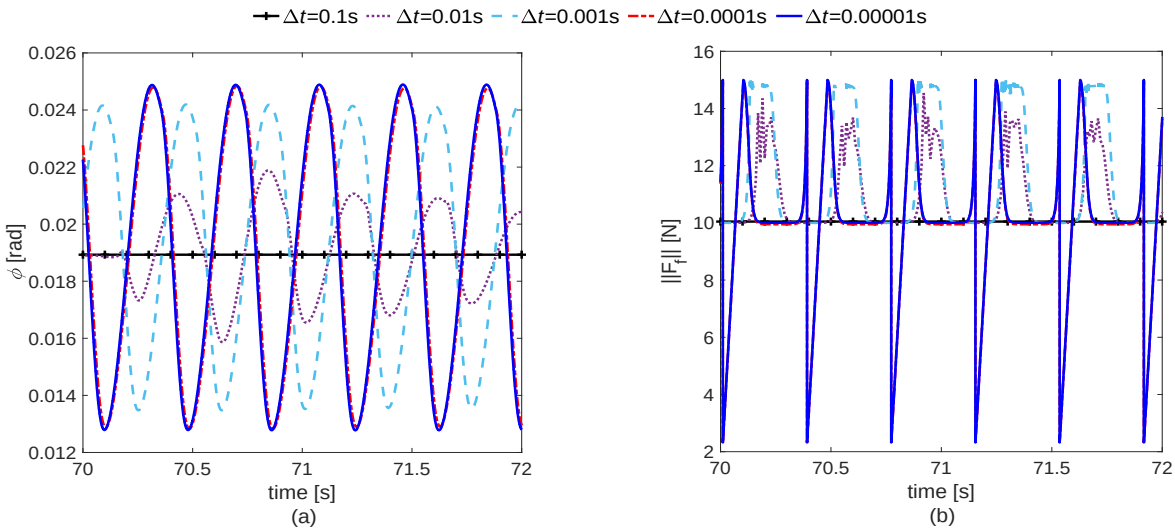

Fig. 5 The steady-state responses of ϕ and $\|\mathbf{F}_f\|$ calculated by the AEOM method with various time steps.

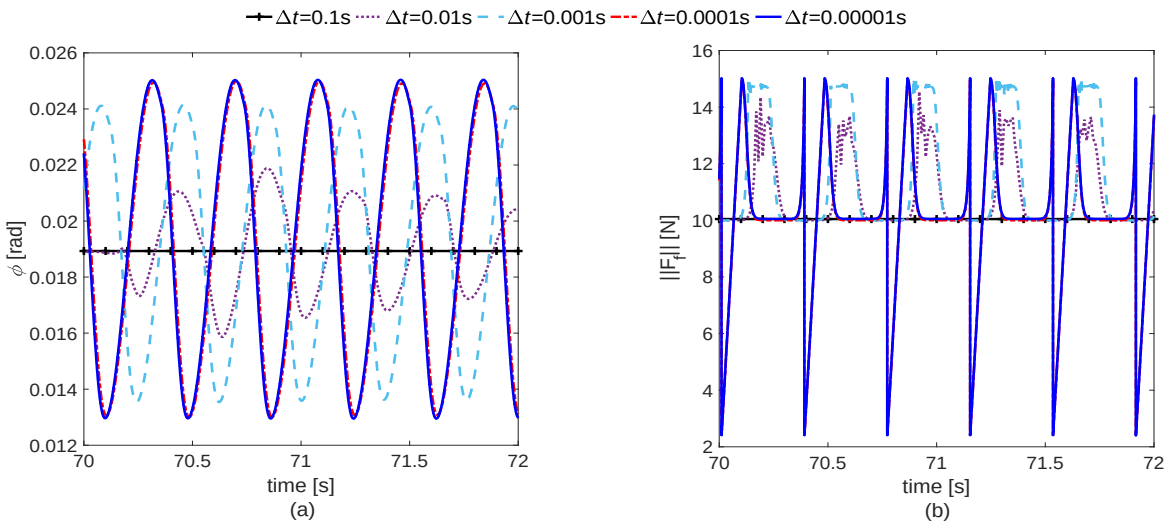

Fig. 6 The steady-state responses of ϕ and $\|\mathbf{F}_\mathrm{f}\|$ calculated by the NAEOM method with various time steps.

Table 2 The computation time of transient dynamic responses (0~100s) by the two numerical methods

Δt	the AEOM method	the NAEOM method
0.1s	0.08s	0.08s
0.01s	0.49s	0.49s
0.001s	3.46s	958.15s
0.0001s	31.36s	9,581.69s
0.00001s	406.53s	95,814.03s

4.2.2 The bi-stability in the system dynamics

A bi-stability phenomenon is also found in this frictional system. Fig. 7 exhibits the time-history responses of ϕ and ψ for three different values of Ω and $N = 50\mathrm{N}$, $\mu_\mathrm{k} = 0.2$, $\Delta\mu = 0.1$, $\alpha = 5$ acquired from two different sets of initial conditions, i.e., one far from the equilibrium point and the other near the equilibrium point. It is observed that when $\Omega = 5\mathrm{rad/s}$, the dynamic responses from two different initial conditions will approach the same stick-slip oscillation; when $\Omega = 12\mathrm{rad/s}$, the dynamic responses from both initial conditions will approach the equilibrium point; when $\Omega = 8.5\mathrm{rad/s}$, one set of initial condition leads to a stick-slip oscillation, the other leads to the equilibrium point in the steady state. The above results indicate the coexistence of two stable steady-state responses for certain values of operating parameters, i.e., bi-stability.

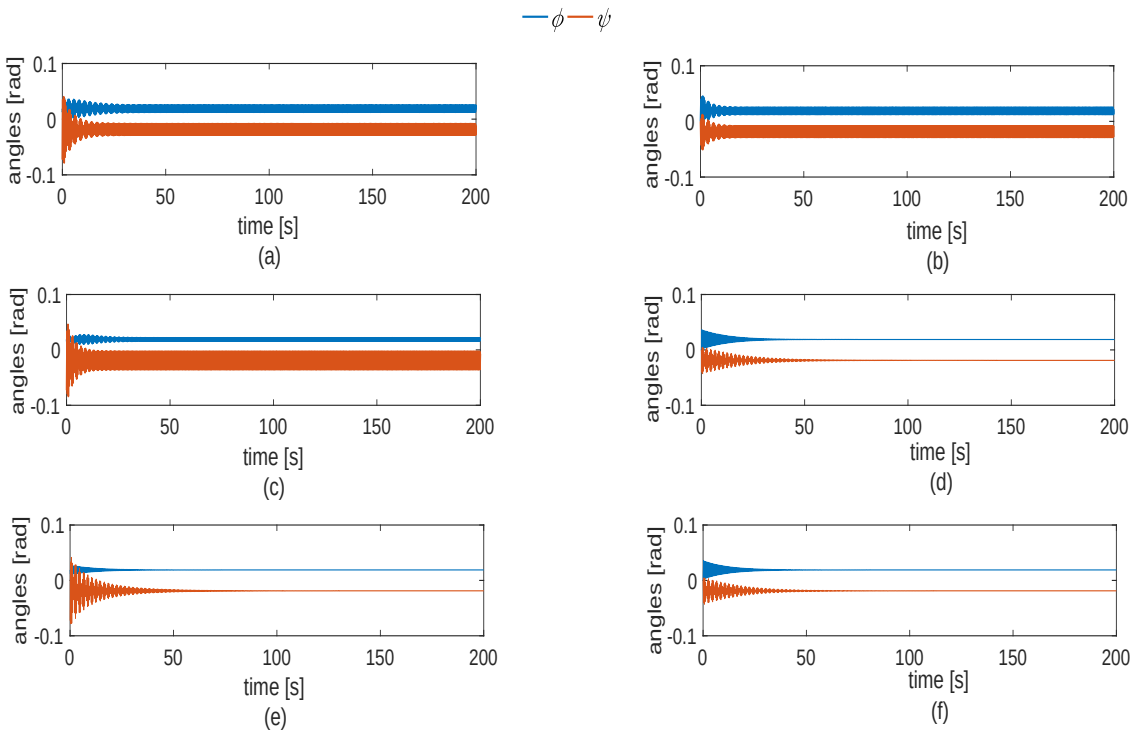

Fig. 7 The time responses of ϕ and ψ when $\Omega = 5\text{rad/s}$ (a)(b), $\Omega = 8.5\text{rad/s}$ (c)(d), $\Omega = 12\text{rad/s}$ (e)(f) and $\mu_k = 0.2$, $\Delta\mu = 0.1$, $\alpha = 5$, $N = 50\text{N}$ from two different initial conditions: (a)(c)(e) far from the equilibrium point and (b)(d)(f) near the equilibrium point.

According to the types of steady-state responses, the parameter plane of (N, Ω) can be divided into three different regions I, II, III that contain the values of the operating parameters leading to a single stable stick-slip oscillation, coexistence of a stable stick-slip oscillation and a stable equilibrium point, and a single stable equilibrium point, respectively, as displayed in Fig. 8.

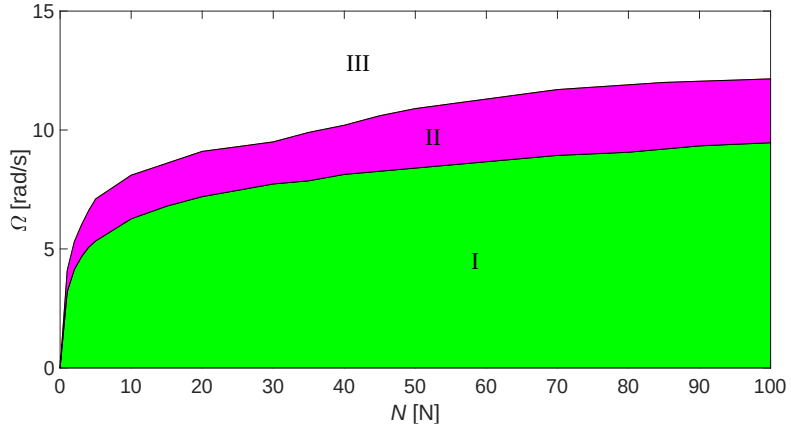

Fig. 8 The ranges of (N, Ω) leading to three different types of steady-state responses.

Fig. 8 indicates that a low Ω or a high N promotes stick-slip oscillation. Therefore, if undesirable stick-slip oscillation occurs in some engineering applications such as automotive brake noise, these two factors can be used to hinder or disrupt stick-slip oscillation. A recent study by the authors' team found a time-varying normal force could have a profound influence on stick-slip vibration behaviour [50].

4.2.3 The characteristics of the stick-slip oscillations

It has been revealed in Section 4.2.2 that the system has stable stick-slip oscillations for certain values of the operating parameters. To have a better understanding of the system dynamics, the characteristics of the stick-slip oscillations will be further analysed.

First of all, the ranges of the operating parameters where the stick-slip oscillation can occur, i.e., the sum of the parameter regions I and II as shown in Fig. 8, for four dynamic models, are compared. These four models are the present model (Model 1), the model in which the two rigid plates have the rotational motion around the centres and the translational motion in the fixed direction of x_1, x_2 (Model 2), the model in which the two rigid plates have the rotational motion around the centres and the translational motion in the fixed direction of y_1, y_2 (Model 3), and the reduced model with only rotational motion for the two rigid plates (Model 4). The results of the parameter ranges in which the stick-slip oscillation can occur for the four dynamic models with $\mu_k = 0.2$, $\Delta\mu = 0.1$, $\alpha = 5$ are presented in Fig. 9 as the domains below corresponding curves. It is shown that the 'stick-slip' domain for the reduced model with only rotational motion is significantly smaller than those for other three models, which demonstrates that the addition of the translational motion increases the possibility of occurrence of stick-slip oscillation in the system.

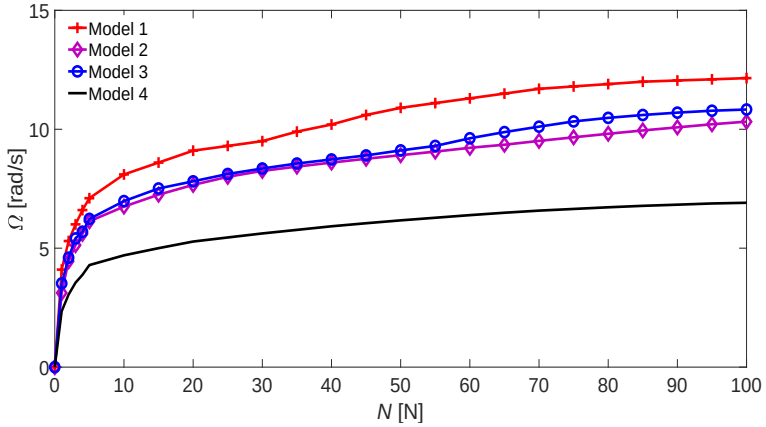

Fig. 9 The ranges of the operating parameters in which stick-slip vibration can occur

Then, as with many previous works on friction-induced vibration [51-57], the focus of investigation will be on the characteristics of the circumferential oscillation of the driven upper rigid plate, i.e., the response of ϕ. In Fig. 10, the steady-state stick-slip oscillations at different normal forces with $\mu_k = 0.2$, $\Delta\mu = 0.1$, $\alpha = 5$, $\Omega = 0.5\text{rad/s}$ are exhibited in terms of time histories, phase plots and frequency spectra of ϕ. It is seen that by varying N, distinct dynamic responses are produced. A periodic oscillation of almost only one amplitude peak at the frequency of 1.46Hz is shown in Fig. 10(a), indicating the vibration of ϕ is nearly harmonic at $N = 30\text{N}$. When $N = 50\text{N}, 70\text{N}, 90\text{N}, 110\text{N}$, the responses of ϕ are also periodic but not harmonic, with the fundamental frequency of 0.99Hz, 0.78Hz, 0.58Hz, 0.43Hz and corresponding superharmonics, respectively, as shown in Fig. 10(b)-(e). When

$N = 120$N, however, ϕ is non-periodic, as shown in Fig. 10(f). This example demonstrates the rich bifurcation behaviours of the stick-slip oscillations of the system with parameter variations.

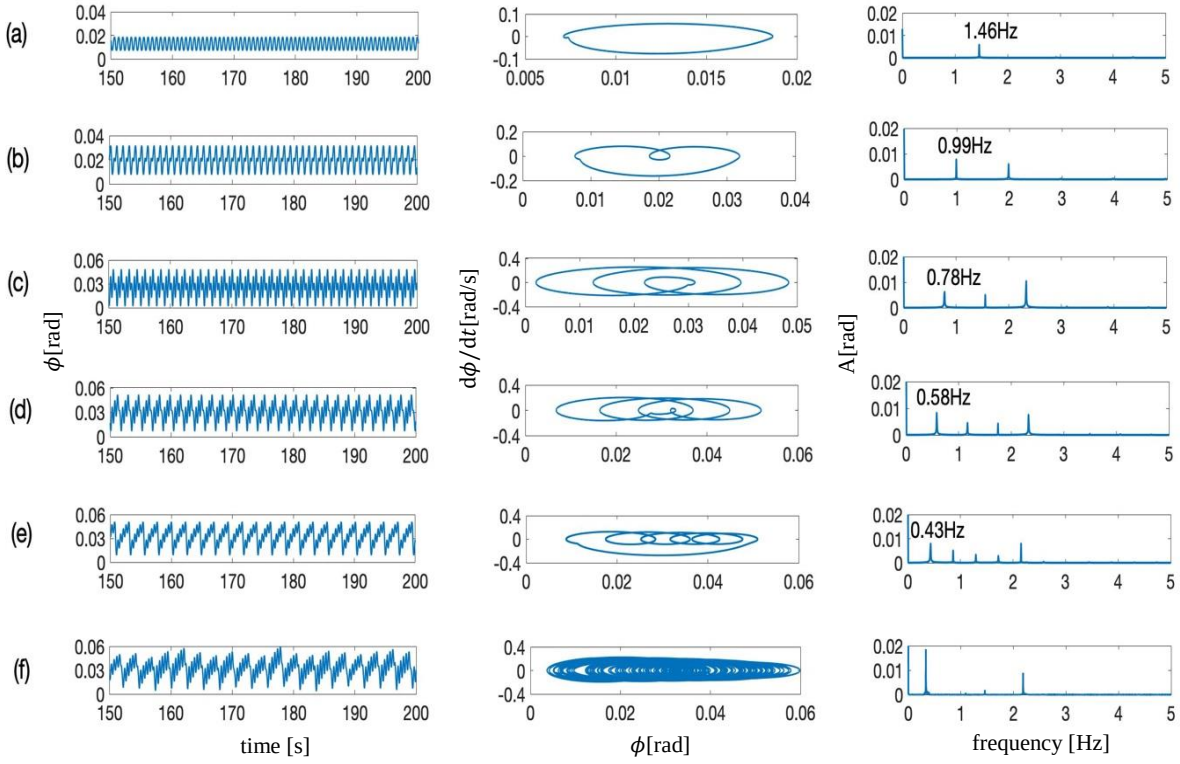

Fig. 10 Time histories, phase plots and frequency spectra of ϕ at different normal forces: (a) $N = 30$N, (b) $N = 50$N, (c) $N = 70$N, (d) $N = 90$N, (e) $N = 110$N and (f) $N = 120$N.

Besides, the direction of relative motion between the two plates during vibration is examined. Fig. 11 exhibits the variations of the angle of $\mathbf{v}_r$ relative to the gross circumferential direction during vibration at $N = 30$N and $N = 120$N. The angle between the direction of relative motion and the circumferential direction varies periodically within $[5^\circ, 15^\circ]$ at $N = 30$N and non-periodically within $[0^\circ, 20^\circ]$ at $N = 120$N, as exhibited by the blue solid curves. In contrast, the relative motion between the two plates is always along the fixed circumferential direction when the centres of the two rigid plates are rigidly constrained, which is represented by the red dashed lines in Fig. 11. The variation of the direction of relative motion also acts as a significant indicator of the rich dynamics of the system.

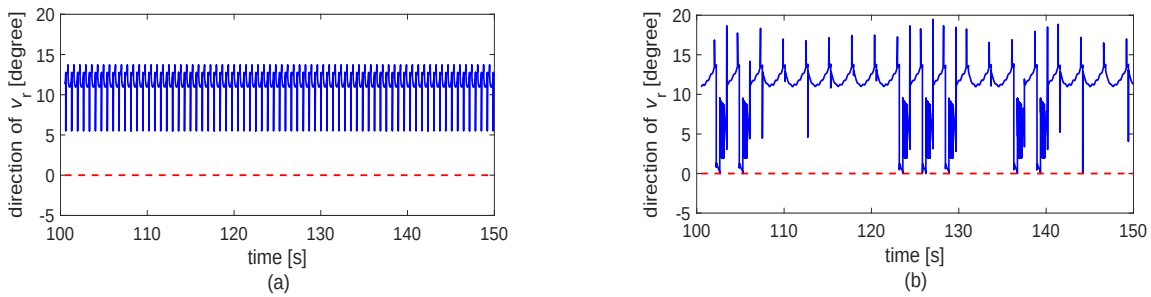

Fig. 11 The angle of relative motion relative to the gross circumferential direction during vibration: (a)) $N = 30$N and (b) $N = 120$N.

To get a complete picture of the bifurcation behaviours of ϕ, the bifurcation diagrams using the operating parameters (N, Ω) and friction parameters ($\Delta\mu$, α) as the control parameters, in which the peak values of ϕ in the steady state are shown, are presented in Fig. 12 and Fig. 13, respectively. Fig. 12 shows that the bifurcations of ϕ with the variations of operating parameters are monotonous, namely, the response of ϕ changes from periodic stick-slip oscillation with growing period to non-periodic stick-slip oscillation with the increase of N and decrease of Ω. However, the monotonicity is not displayed in the bifurcations with the variations of the friction parameters. By increasing $\Delta\mu$, the response of ϕ changes from periodic oscillation to non-periodic oscillation and eventually back to periodic oscillation. By increasing α, the response of ϕ changes from periodic oscillation to non-periodic oscillation, and then back to periodic oscillation and non-periodic oscillation in turn, and eventually back to periodic oscillation.

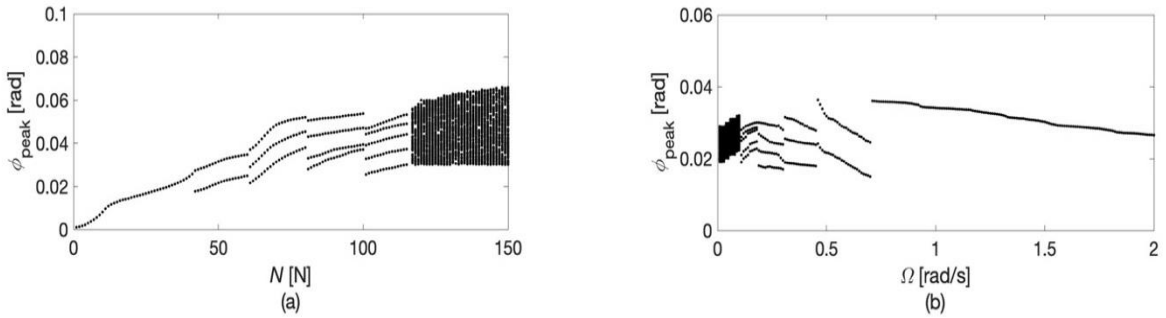

Fig. 12 Bifurcation diagrams of ϕ using N ($\Omega = 0.5\text{rad/s}$) (a) and Ω ($N = 50\text{N}$) (b) as the control parameter. ($\mu_\text{k} = 0.2$, $\Delta\mu = 0.1$, $\alpha = 5$).

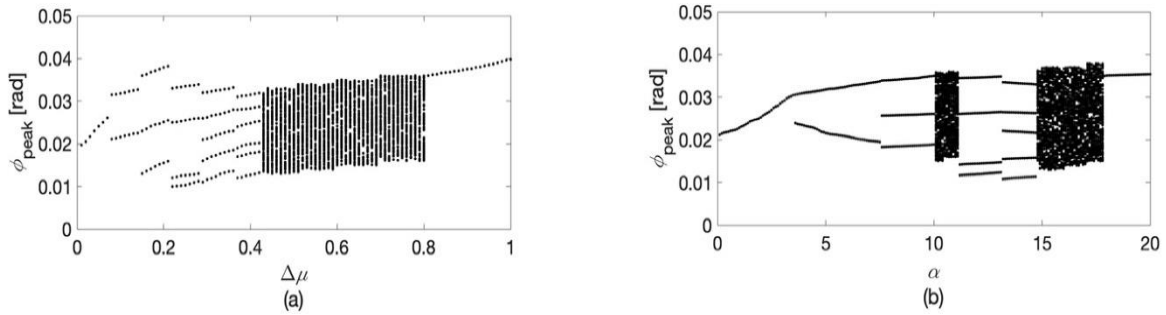

Fig. 13 Bifurcation diagrams of ϕ using $\Delta\mu$ ($\alpha = 5$) (a) and α ($\Delta\mu = 0.1$) (b) as the control parameter. ($\mu_\text{k} = 0.2$, $N = 50\text{N}$, $\Omega = 0.5\text{rad/s}$).

In comparison, Fig. 14 gives the bifurcation diagrams of ϕ with the variations of N and Ω for other three dynamic models. It is observed that for the two models with the rotational motion and the translational motion in the fixed direction for the rigid plates, periodic stick-slip oscillations with different periods (or frequencies) appear as N or Ω varies. For the reduced model with only rotational motion for the rigid plates, however, no bifurcation appears, i.e, ϕ has periodic stick-slip oscillation with unchanged period (or frequency) with the variation of N or Ω. In Fig. 15, a representation of the response in the reduced model in which the two rigid plates undergo only rotational motion is shown. The comparison between the results in Fig. 12 and Fig. 14 demonstrates that the addition of the two-

dimensional translational motion for both rigid plates greatly enhances the variability of the frequency spectra (the periodicity) of the response of ϕ within the operating range.

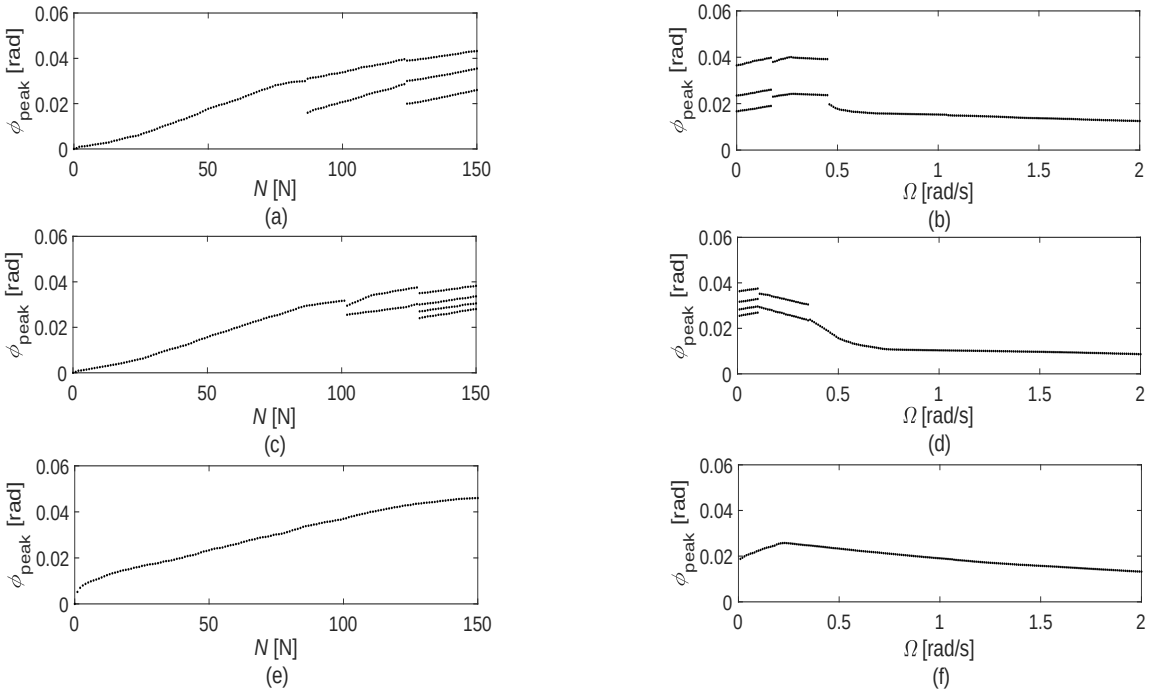

Fig. 14 Bifurcation diagrams of ϕ with the variations of N ($\Omega = 0.5\text{rad/s}$) and Ω ($N = 50\text{N}$) in the model in which the two rigid plates have the rotational motion around the centres and the translational motion in the fixed direction of x_1, x_2 (a)(b) and y_1, y_2 (c)(d) and the two rigid plates have no translational motion but only rotational motion (e)(f). ($\mu_\text{k} = 0.2$, $\Delta\mu = 0.1$, $\alpha = 5$).

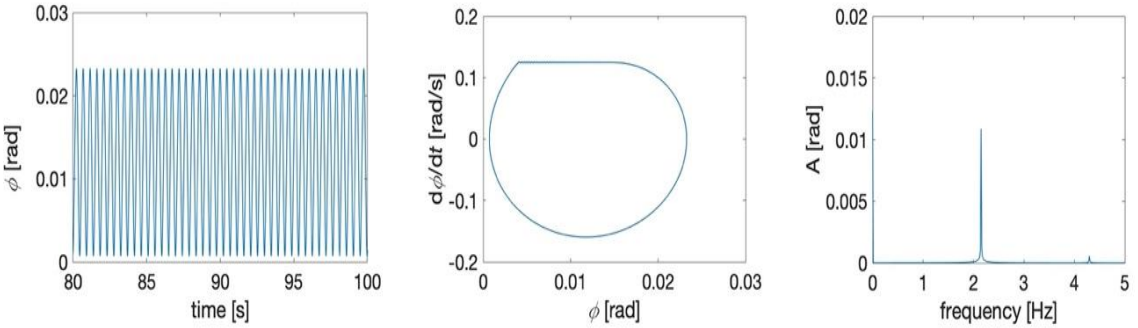

Fig. 15 A representation of the response of ϕ in the reduced model where the two rigid plates undergo only rotational motion

In another aspect, an index is defined to measure the intensity of oscillation in the steady state, that is,

$$I = \frac{\sqrt{\int_T (X - X_\text{e})^2 \text{d}t}}{T} \tag{16}$$

where X represents a response of the system, X_e is the value of the equilibrium point, T is a time period in the steady state. Fig. 16(a) and (b) show the intensity of oscillation of $r\phi$ in the reduced model and

the model studied in this paper, respectively, which indicate that the addition of the two-dimensional translational motion for both rigid plates has no significant effect on the intensity of oscillation of $r\phi$. Besides, the intensity of oscillation of the translational motion of the upper rigid plate is illustrated in Fig. 16(c), which has the same-order magnitude as that of $r\phi$, therefore close attention should also be paid to the amplitudes of the oscillations of components that seem not to be in the principal direction of relative motion.

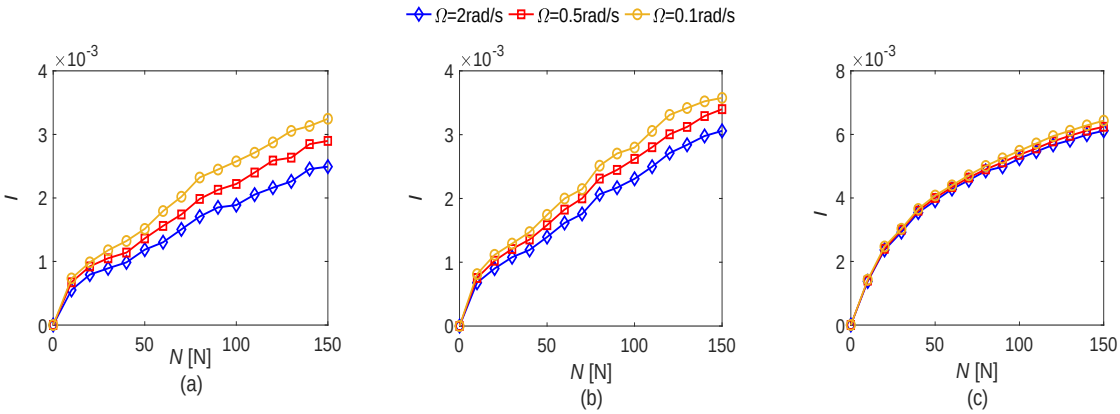

Fig. 16 The intensity of oscillation of system responses: (a) $r\phi$ in the reduced model, (b) $r\phi$ in the model studied in this paper, (c) the translational motion of the upper rigid plate.

5. Conclusions

This paper presents a study of the friction-induced planar vibration of two elastically constrained circular rigid plates in sliding friction contact. The coupling of the translational motion with the rotational motion for both rigid plates results in direction variation of the relative motion and friction force that will usually be not along the circumferential direction, and thus produces nonlinear kinematics of contact and complicates the dynamics of the friction-excited system. The system dynamics consists of two distinct states of motion, i.e., slip and stick. Two methods are proposed to determine the values of the state variables and friction force in the state of stick, which cannot be directly acquired from the integration of the equations of motion because the friction force during sticking is a reaction force enforcing zero relative velocity rather than explicitly expressed as a function of the state variables. The accuracy and efficiency of the two numerical methods for the calculation of the transient dynamic responses of the system are examined. Based on the observations from the numerical study, the following conclusions can be drawn,

1. The equilibrium point of the system is unstable at a sufficiently low rotational speed of lower rigid plate (Ω) and large normal force (N). In addition, the increase of $\Delta\mu$ and α (parameters in the friction law) expands and narrows the range of operating parameters (N, Ω) leading to unstable equilibrium points, respectively. Besides, the nonlinear kinematics of contact brought about by the coupling of

translational motion and rotational motion of the two rigid plates promotes the occurrence of dynamic instability.

2. Bi-stability occurs for a certain range of values of operating parameters. The plane of operating parameters can be divided into three different regions that contain the values leading to a single stable stick-slip oscillation, coexistence of a stable stick-slip oscillation and a stable equilibrium point, and a single stable equilibrium point, respectively.

3. The frequency spectra (the periodicity) of the circumferential oscillation of the driven upper rigid plate, i.e., the response of ϕ, in the present model with the coupling of the two-dimensional translational motion and the rotational motion around the centres for the two rigid plates turn out to experience higher degree of variability within the operating range than that in the reduced model where the two rigid plates have no translational motion but only rotational motion.

4. The inclusion of the translational motion for both rigid plates has no significant effect on the intensity of oscillation of ϕ. Besides, close attention should also be paid to the amplitudes of the oscillations of components that seem not to be in the principal direction of relative motion in the research of friction-induced vibration of mechanical systems.

.

Appendix

The components b_i $(i = 1,2,3,4,5,6)$ in Eq. (14) are,

$$b_1 = -\frac{N(y_1 - y_2 + r\sin\phi)\left[\mu_\mathrm{k} + (\mu_\mathrm{s} - \mu_\mathrm{k})\mathrm{e}^{-\alpha\Omega\sqrt{(y_1-y_2+r\sin\phi)^2+(x_1-x_2+r\cos\phi)^2}}\right]}{\sqrt{(y_1 - y_2 + r\sin\phi)^2 + (x_1 - x_2 + r\cos\phi)^2}},$$

$$b_2 = \frac{N(x_1 - x_2 + r\cos\phi)\left[\mu_\mathrm{k} + (\mu_\mathrm{s} - \mu_\mathrm{k})\mathrm{e}^{-\alpha\Omega\sqrt{(y_1-y_2+r\sin\phi)^2+(x_1-x_2+r\cos\phi)^2}}\right]}{\sqrt{(y_1 - y_2 + r\sin\phi)^2 + (x_1 - x_2 + r\cos\phi)^2}},$$

$$b_3 = -b_1,\ b_4 = -b_2,$$

$$b_5 = \frac{Nr[(y_1 - y_2 + r\sin\phi)\sin\phi + (x_1 - x_2 + r\cos\phi)\cos\phi]\left[\mu_\mathrm{k} + (\mu_\mathrm{s} - \mu_\mathrm{k})\mathrm{e}^{-\alpha\Omega\sqrt{(y_1-y_2+r\sin\phi)^2+(x_1-x_2+r\cos\phi)^2}}\right]}{\sqrt{(y_1 - y_2 + r\sin\phi)^2 + (x_1 - x_2 + r\cos\phi)^2}},$$

$$b_6 = -N\sqrt{(y_1 - y_2 + r\sin\phi)^2 + (x_1 - x_2 + r\cos\phi)^2}\left[\mu_\mathrm{k} + (\mu_\mathrm{s} - \mu_\mathrm{k})\mathrm{e}^{-\alpha\Omega\sqrt{(y_1-y_2+r\sin\phi)^2+(x_1-x_2+r\cos\phi)^2}}\right]. \quad \text{(A.1)}$$

The mass matrix, damping matrix and stiffness matrix of the linearized system in Eq. (16) are,

$$\mathbf{M}_\mathrm{L} = \mathrm{diag}\left(m_\mathrm{p}, m_\mathrm{p}, J_\mathrm{p}, m_\mathrm{d}, m_\mathrm{d}, J_\mathrm{d}\right),\ \mathbf{C}_\mathrm{L} = \left(C_{ij}\right)_{6\times6} = {\mathbf{C}_\mathrm{L}}^\mathrm{T},\ \mathbf{K}_\mathrm{L} = \left(K_{ij}\right)_{6\times6} \neq {\mathbf{K}_\mathrm{L}}^\mathrm{T},\ 1 \le i \le 6,\ 1 \le j \le 6 \quad \text{(A.2)}$$

where,

$$C_{11} = c_\mathrm{px} - N\left[\left(\frac{\alpha\Delta\mu\mathrm{e}^{-\alpha v_\mathrm{re}}}{{v_\mathrm{re}}^2} + \frac{\mu_\mathrm{e}}{{v_\mathrm{re}}^3}\right){v_\mathrm{re}^x}^2 - \frac{\mu_\mathrm{e}}{v_\mathrm{re}}\right],\ C_{21} = -N v_\mathrm{re}^x v_\mathrm{re}^y\left(\frac{\alpha\Delta\mu\mathrm{e}^{-\alpha v_\mathrm{re}}}{{v_\mathrm{re}}^2} + \frac{\mu_\mathrm{e}}{{v_\mathrm{re}}^3}\right),\ C_{31} = c_\mathrm{px} - C_{11},$$

$$C_{41} = -C_{21},\ C_{51} = Nr\left[\left(\frac{\alpha\Delta\mu e^{-\alpha v_{re}}}{{v_{re}}^2} + \frac{\mu_e}{{v_{re}}^3}\right)\left(\sin(\phi_e){v_{re}^x}^2 - \cos(\phi_e)v_{re}^x v_{re}^y\right) - \mu_e\frac{\sin(\phi_e)}{v_{re}}\right],$$

$$C_{61} = N\left[\left(\frac{\alpha\Delta\mu e^{-\alpha v_{re}}}{{v_{re}}^2} + \frac{\mu_e}{{v_{re}}^3}\right)\frac{X_e v_{re}^x v_{re}^y - Y_e {v_{re}^x}^2}{{v_{re}}^2} + \mu_e\frac{Y_e}{v_{re}}\right], C_{22} = c_{py} - N\left[\left(\frac{\alpha\Delta\mu e^{-\alpha v_{re}}}{{v_{re}}^2} + \frac{\mu_e}{{v_{re}}^3}\right){v_{re}^y}^2 - \frac{\mu_e}{v_{re}}\right],$$

$$C_{32} = -C_{21}, C_{42} = c_{py} - C_{22}, C_{52} = Nr\left[\left(\frac{\alpha\Delta\mu e^{-\alpha v_{re}}}{{v_{re}}^2} + \frac{\mu_e}{{v_{re}}^3}\right)\left(\sin(\phi_e)v_{re}^x v_{re}^y - \cos(\phi_e){v_{re}^y}^2\right) + \mu_e\frac{\cos(\phi_e)}{v_{re}}\right],$$

$$C_{62} = N\left[\left(\frac{\alpha\Delta\mu e^{-\alpha v_{re}}}{{v_{re}}^2} + \frac{\mu_e}{{v_{re}}^3}\right)\frac{X_e {v_{re}^y}^2 - Y_e v_{re}^x v_{re}^y}{{v_{re}}^2} - \mu_e\frac{X_e}{v_{re}}\right], C_{33} = c_{dx} - C_{31}, C_{43} = C_{21}, C_{53} = -C_{51}, C_{63} = -C_{61},$$

$$C_{44} = c_{dy} - C_{42}, C_{54} = -C_{52}, C_{64} = -C_{62}, C_{55} = c_{p\varphi} - Nr\left[\left(\frac{\alpha\Delta\mu e^{-\alpha v_{re}}}{{v_{re}}^2} + \frac{\mu_e}{{v_{re}}^3}\right)(r\cos(\phi_e)v_{re}^y - r\sin(\phi_e)v_{re}^x)^2 - \frac{\mu_e}{v_{re}}\right],$$

$$C_{65} = Nr\left[\left(\frac{\alpha\Delta\mu e^{-\alpha v_{re}}}{{v_{re}}^2} + \frac{\mu_e}{{v_{re}}^3}\right)\left(\cos(\phi_e)v_{re}^y - \sin(\phi_e)v_{re}^x\right)\left(X_e v_{re}^y - Y_e v_{re}^x\right) - \mu_e\frac{(\sin(\phi_e)Y_e + \cos(\phi_e)X_e)}{v_{re}}\right],$$

$$C_{66} = c_{d\psi} - N\left[\left(\frac{\alpha\Delta\mu e^{-\alpha v_{re}}}{{v_{re}}^2} + \frac{\mu_e}{{v_{re}}^3}\right)\left(X_e v_{re}^y - Y_e v_{re}^x\right)^2 - \mu_e\frac{{X_e}^2 + {Y_e}^2}{v_{re}}\right].$$

and there is $C_{ji} = C_{ij}(2 \le i \le 6, 1 \le j \le 5,\ j < i)$ as the matrix $\mathbf{C}_L$ is symmetric. The entries in the matrix $\mathbf{K}_L$ are,

$$K_{11} = k_{px} + N\Omega\left(\frac{\alpha\Delta\mu e^{-\alpha v_{re}}}{{v_{re}}^2} + \frac{\mu_e}{{v_{re}}^3}\right)v_{re}^x v_{re}^y,\ K_{12} = -N\Omega\left[\left(\frac{\alpha\Delta\mu e^{-\alpha v_{re}}}{{v_{re}}^2} + \frac{\mu_e}{{v_{re}}^3}\right){v_{re}^x}^2 - \frac{\mu_e}{v_{re}}\right], K_{13} = k_{px} - K_{11},$$

$$K_{14} = -K_{12}, K_{15} = -N\Omega r\left[\left(\frac{\alpha\Delta\mu e^{-\alpha v_{re}}}{{v_{re}}^2} + \frac{\mu_e}{{v_{re}}^3}\right)\left(\cos(\phi_e){v_{re}^x}^2 + \sin(\phi_e)v_{re}^x v_{re}^y\right) - \mu_e\frac{\cos(\phi_e)}{v_{re}}\right], K_{16} = 0,$$

$$K_{21} = N\Omega\left[\left(\frac{\alpha\Delta\mu e^{-\alpha v_{re}}}{{v_{re}}^2} + \frac{\mu_e}{{v_{re}}^3}\right){v_{re}^y}^2 - \frac{\mu_e}{v_{re}}\right], K_{22} = k_{py} - N\Omega\left(\frac{\alpha\Delta\mu e^{-\alpha v_{re}}}{{v_{re}}^2} + \frac{\mu_e}{{v_{re}}^3}\right)v_{re}^x v_{re}^y, K_{23} = -K_{21},$$

$$K_{24} = -K_{13}, K_{25} = -N\Omega r\left[\left(\frac{\alpha\Delta\mu e^{-\alpha v_{re}}}{{v_{re}}^2} + \frac{\mu_e}{{v_{re}}^3}\right)\left(\sin(\phi_e){v_{re}^y}^2 + \cos(\phi_e)v_{re}^x v_{re}^y\right) - \mu_e\frac{\sin(\phi_e)}{v_{re}}\right], K_{26} = 0,$$

$$K_{31} = K_{13}, K_{32} = -K_{12}, K_{33} = k_{dx} - K_{13}, K_{34} = -K_{14}, K_{35} = -K_{15}, K_{36} = 0,$$

$$K_{41} = -K_{21}, K_{42} = K_{24}, K_{43} = -K_{23}, K_{44} = k_{dy} - K_{24}, K_{45} = -K_{25}, K_{46} = 0,$$

$$K_{51} = N\Omega r\left[\left(\frac{\alpha\Delta\mu e^{-\alpha v_{re}}}{{v_{re}}^2} + \frac{\mu_e}{{v_{re}}^3}\right)\left(\cos(\phi_e){v_{re}^y}^2 - \sin(\phi_e)v_{re}^x v_{re}^y\right) - \mu_e\frac{\cos(\phi_e)}{v_{re}}\right],$$

$$K_{52} = -N\Omega r\left[\left(\frac{\alpha\Delta\mu e^{-\alpha v_{re}}}{{v_{re}}^2} + \frac{\mu_e}{{v_{re}}^3}\right)\left(\cos(\phi_e)v_{re}^x v_{re}^y - \sin(\phi_e){v_{re}^x}^2\right) + \mu_e\frac{\sin(\phi_e)}{v_{re}}\right], K_{53} = -K_{51}, K_{54} = -K_{52},$$

$$K_{55} = k_{p\varphi} - N\Omega r\left(\frac{\alpha\Delta\mu e^{-\alpha v_{re}}}{{v_{re}}^2} + \frac{\mu_e}{{v_{re}}^3}\right)\left(\cos(\phi_e)v_{re}^x + \sin(\phi_e)v_{re}^y\right)\left(-\sin(\phi_e)v_{re}^x + \cos(\phi_e)v_{re}^y\right), K_{56} = 0,$$

$$K_{61} = -N\Omega\left[\left(\frac{\alpha\Delta\mu e^{-\alpha v_{re}}}{{v_{re}}^2} + \frac{\mu_e}{{v_{re}}^3}\right)\left(X_e {v_{re}^y}^2 - Y_e v_{re}^x v_{re}^y\right) - 2\mu_e\frac{X_e}{v_{re}}\right], K_{63} = -K_{61},$$

$$K_{62} = N\Omega\left[\left(\frac{\alpha\Delta\mu e^{-\alpha v_{re}}}{{v_{re}}^2} + \frac{\mu_e}{{v_{re}}^3}\right)\left(X_e v_{re}^x v_{re}^y - Y_e {v_{re}^x}^2\right) + 2\mu_e\frac{Y_e}{v_{re}}\right], K_{64} = -K_{62},$$

$$K_{65} = N\Omega r\left[\left(\frac{\alpha\Delta\mu e^{-\alpha v_{re}}}{{v_{re}}^2} + \frac{\mu_e}{{v_{re}}^3}\right)(\cos(\phi_e)v_{re}^x + \sin(\phi_e)v_{re}^y)(X_e v_{re}^y - Y_e v_{re}^x) + 2\mu_e\frac{\cos(\phi_e)Y_e - \sin(\phi_e)X_e}{v_{re}}\right], K_{66} = k_{d\psi}.$$

in which,

$$X_e = x_{1e} - x_{2e} + r\cos(\phi_e), Y_e = y_{1e} - y_{2e} + r\sin(\phi_e), v_{re}^x = \Omega Y_e, v_{re}^y = -\Omega X_e,$$

$$v_{\mathrm{re}} = \Omega\sqrt{{X_{\mathrm{e}}}^2 + {Y_{\mathrm{e}}}^2}, \mu_{\mathrm{e}} = \mu_{\mathrm{k}} + \Delta\mu \mathrm{e}^{-\alpha v_{\mathrm{re}}}.$$

Authorship contribution statement

Ningyu Liu: Conceptualization, Formal analysis, Investigation, Methodology, Validation, Writing - original draft, Writing - review & editing. **Huajiang Ouyang**: Conceptualization, Methodology, Project administration, Writing - original draft, Writing - review & editing.

Acknowledgements

The first author is sponsored by a University of Liverpool and China Scholarship Council joint scholarship.

Statement on Conflict of Interest

The authors declare that they have no conflict of interest.

References

[1] Cremer, L., Hall, D.E., The physics of the violin, Am. J. Phys. 54 (1986) 285.

[2] Cai, L., Songag, G., Joint stick-slip friction compensation of robot manipulators by using smooth robust controllers, J. Robot. Syst. 11**(**6) (1994) 451-470.

[3] Ibrahim, R.A., Friction-induced vibration, chatter, squeal, and chaos—part I: mechanics of contact and friction, Appl. Mech. Rev. 47 (1994) 209-226.

[4] Leine, R.I., Van Campen, D.H., Keultjes, W.J.G., Stick-slip whirl interaction in drill-string dynamics, J. Vib. Acoust. 124(2) (2002) 209-220.

[5] Koenen, A., Sanon, A., Tribological and vibroacoustic behavior of a contact between rubber and glass (application to wiper blade), Tribol. Int. 40(10-12) (2007) 1484-1491.

[6] Ibrahim, R.A., Friction-induced vibration, chatter, squeal, and chaos. Part II: dynamics and modelling, Appl. Mech. Rev. 47(7) (1994) 227–253.

[7] Sinclair, D., Manville, N., Frictional vibrations, J. Appl. Mech. T. ASME. 22 (1955) 13-207.

[8] Feeny, B., Guran, A.S., Hinrichs, N., Popp, K., A historical review on dry friction and stick-slip phenomena, Appl. Mech. Rev. 51(5) (1998) 321-341.

[9] Sinou, J.J., Thouverez, F., Jezequel, L., Analysis of friction and instability by the centre manifold theory for a non-linear sprag-slip model, J. Sound Vib. 265(3) (2003) 527-559.

[10] Sinou, J.J., Jézéquel, L., Mode coupling instability in friction-induced vibrations and its dependency on system parameters including damping, Eur. J. Mech. A-Solid 26(1) (2007) 106-122.

[11] Oden, J.T., Martins, J.A.C., Models and computational methods for dynamic friction phenomena, Comput. Method Appl. M. 52**(**1) (1985) 527-634.

[12] Popp, K., Hinrichs, N., Oestreich, M., Dynamical behaviour of a friction oscillator with simultaneous self and external excitation, Sadhana 20(2-4) (1995) 627-654.

[13] Popp, K., Hinrichs, N., Oestreich, M., Analysis of a self excited friction oscillator with external excitation, Dynamics With Friction: Modeling, Analysis And Experiment: (Part I) (1996) 1-35.

[14] Li, Z., Ouyang, H., Guan, Z., Friction-induced vibration of an elastic disc and a moving slider with separation and reattachment, Nonlinear Dyn. 87(2) (2017) 1045-1067.

[15] Liu, N., Ouyang, H., Friction-induced vibration of a slider on an elastic disc spinning at variable speeds, Nonlinear Dyn. 98(1) (2019) 39-60.

[16] Lin, W., Chavez, J.P., Liu, Y., Yang, Y., Kuang, Y., Stick-slip suppression and speed tuning for a drill-string system via proportional-derivative control, Appl. Math. Model. 82 (2020) 487-502.

[17] Hoffmann, N., Gaul, L., A sufficient criterion for the onset of sprag-slip oscillations, Arch. Appl. Mech. 73(9-10) (2004) 650-660.

[18] Keitzel, H., Hoffmann, N., Influence of the contact model on the onset of sprag- slip, PAMM: Proceedings in Applied Mathematics and Mechanics 6 (2006) 311- 312.

[19] Hoffmann, N., Fischer, M., Allgaier, R., Gaul, L., A minimal model for studying properties of the mode-coupling type instability in friction induced oscillations, Mech. Res. Commun. 29(4) (2002) 197-205.

[20] Hoffmann, N., Gaul, L., Effects of damping on mode-coupling instability in friction induced oscillations, ZAMM-Journal of Applied Mathematics and Mechanics 83(8) (2003) 524-534.

[21] Hervé, B., Sinou, J.J., Mahé, H., Jezequel, L., Analysis of squeal noise and mode coupling instabilities including damping and gyroscopic effects, Eur. J. Mech. A-Solid 27(2) (2008) 141-160.

[22] Elmaian, A., Gautier, F., Pezerat, C., Duffal, J.M., How can automotive friction- induced noises be related to physical mechanisms? Appl. Acoust. 76 (2014) 391-401.

[23] Liu, N., Ouyang, H., Suppression of friction-induced-vibration in MDoF systems using tangential harmonic excitation, Meccanica 55 (2020) 1525-1542.

[24] Popp, K., Stelter, P., Stick–slip vibrations and chaos, Philosophical Transactions: Physical Sciences and Engineering 332(1624) (1990) 89-105.

[25] Li, Y., Feng, Z.C., Bifurcation and chaos in friction-induced vibration, Commun, Nonlinear Sci. 9(6) (2004) 633-647.

[26] Weiss, C., Morlock, M.M., Hoffmann, N.P., Friction induced dynamics of ball joints: Instability and post bifurcation behavior, Eur. J. Mech. A-Solid 45 (2014) 161-173.

[27] Kruse, S., Tiedemann, M., Zeumer, B., Reuss, P., Hetzler, H., Hoffmann, N., The influence of joints on friction induced vibration in brake squeal, J. Sound Vib. 340 (2015) 239-252 .

[28] Wei, D., Song, J., Nan, Y., Zhu, W., Analysis of the stick-slip vibration of a new brake pad with double-layer structure in automobile brake system, Mech. Syst. Signal Pr. 118 (2019) 305-316.

[29] Liu, Y., Lin, W., Chávez, J.P., Sa De, R., Torsional stick-slip vibrations and multistability in drill-strings, Appl. Math. Model. 76 (2019) 545-557.

[30] Pilipchuk, V., Olejnik, P., Awrejcewicz, J., Transient friction-induced vibrations in a 2-DOF model of brakes, J. Sound Vib. 344 (2015) 297–312.

[31] Liu, N., Ouyang, H., Friction-induced vibration considering multiple types of nonlinearities, Nonlinear Dyn. 102 (2020) 2057-2075.

[32] Papangelo, A., Hoffmann, N., Grolet, A., Stender, M., Ciavarella, M., Multiple spatially localized dynamical states in friction-excited oscillator chains, J. Sound Vib. 417 (2018) 56-64.

[33] Kinkaid, N.M., O'Reilly, O.M., Papadopoulos, P., On the transient dynamics of a multi-degree-of-freedom friction oscillator: a new mechanism for disc brake noise, J. Sound Vib. 287(4-5) (2005) 901-917.

[34] Antali, M., Stepan, G., Nonsmooth analysis of three-dimensional slipping and rolling in the presence of dry friction, Nonlinear Dyn. 97 (2019) 1799–1817.

[35] Ma, S., Wang, T., Planar multiple-contact problems subject to unilateral and bilateral kinetic constraints with static Coulomb friction, Nonlinear Dyn. 94 (2018) 99-121.

[36] Charroyer, L., Chiello, O., Sinou, J.J., Self-excited vibrations of a non-smooth contact dynamical system with planar friction based on the shooting method, Int. J. Mech. Sci. 144 (2018) 90-101.

[37] Charroyer, L., Chiello, O., Sinou, J.J., Parametric study of the mode coupling instability for a simple system with planar or rectilinear friction, J. Sound Vib. 384 (2016) 94-112.

[38] Lisowski, B., Retiere, C., Moreno, J.P.G., Olejnik, P., Semiempirical identification of nonlinear dynamics of a two- degree-of-freedom real torsion pendulum with a nonuniform planar stick–slip friction and elastic barriers, Nonlinear Dyn. 100 (2020) 3215-3234.

[39] Xia, F., Modelling of wedge dampers in the presence of two-dimensional dry friction, Vehicle Syst. Dyn. 37 (2002) 565-578.

[40] Sanliturk, K.Y., Ewins, D.J., Modelling two-dimensional friction contact and its application using harmonic balance method, J. Sound Vib. 193(2) (1996) 511-523.

[41] Menq, C.H., Chidamparam, P., Griffin, J.H., Friction damping of two-dimensional motion and its application in vibration control, J. Sound Vib. 144(3) (1991) 427-447.

[42] Marques, F., Flores, P., Claro, J.P., Lankarani, H.M., A survey and comparison of several friction force models for dynamic analysis of multibody mechanical systems, Nonlinear Dyn. 86(3) (2016) 1407-1443.

[43] Pollard, H., Tenenbaum, M., Ordinary differential equations, New York: Harper&Row (1964).

[44] Davis, P.J., Rabinowitz, P., Methods of numerical integration, Courier Corporation (2007).

[45] Misra, S., Wahab, M.F., Patel, D.C., Armstrong, D.W., The utility of statistical moments in chromatography using trapezoidal and Simpson's rules of peak integration, J. Sep. Sci. 42(8) (2019) 1644-1657.

[46] Fornberg, B., Improving the accuracy of the trapezoidal rule, SIAM Review 63(1) (2021) 167-180.

[47] Kwon, S.B., Bathe, K.J., Noh, G., An analysis of implicit time integration schemes for wave propagations, Comput. Struct. 230 (2020) 106188.

[48] Oskouie, M.F., Ansari, R., Rouhi, H., Bending of Euler–Bernoulli nanobeams based on the strain-driven and stress-driven nonlocal integral models: a numerical approach, Acta Mech. Sinica 34(5) (2018) 871-882.

[49] Garrappa, R., Trapezoidal methods for fractional differential equations: Theoretical and computational aspects, Math. Comput. Simulat. 110 (2015) 96-112.

[50] Wang X.C., Wang R.L., Huang B., Mo J.L., Ouyang H., A study of effect of various normal force loading forms on frictional stick-slip vibration, J. Dyn., Monit. Diag., 1(1) (2022), 46-55.

[51] Behrendt, J., Weiss, C., Hoffmann, N.P., A numerical study on stick–slip motion of a brake pad in steady sliding, J. Sound Vib. 330(4) (2011) 636- 651.

[52] Van de Vrande, B.L., Van Campen, D.H., De Kraker, A., An approximate analysis of dry-friction-induced stick–slip vibrations by a smoothing procedure, Nonlinear Dyn. 19(2) (1999) 159-171.

[53] Hetzler, H., On the effect of nonsmooth Coulomb friction on Hopf bifurcations in a 1-DoF oscillator with self-excitation due to negative damping, Nonlinear Dyn. 69(1-2) (2012) 601-614.

[54] Tonazzi, D., Massi, F., Baillet, L., Culla, A., Di Bartolomeo, M., Berthier, Y., Experimental and numerical analysis of frictional contact scenarios: from macro stick–slip to continuous sliding, Meccanica. 50(3) (2015) 649-664.

[55] Leine, R.I., Van Campen, D.H., Bifurcation phenomena in non-smooth dynamical systems, Eur. J. Mech. A-Solid 25(4) (2006) 595-616.

[56] Centea, D., Rahnejat, H., Menday, M.T., Non-linear multi-body dynamic analysis for the study of clutch torsional vibrations (judder), Appl. Math. Model. 25(3) (2001) 177-192.

[57] Papangelo, A., Ciavarella, M., Hoffmann, N., Subcritical bifurcation in a self- excited single-degree-of-freedom system with velocity weakening–strengthening friction law: analytical results and comparison with experiments, Nonlinear Dyn. 90(3) (2017) 2037-2046.